Scanning laser reflectometry of retinal and subretinal tissues

A.E. Elsner, L. Moraes, E. Beausencourt, A. Remky, S.A. Burns, J.J. Weiter, J. P. Walker, G. L. Wing, P. A. Raskauskas and L. M. Kelley

Schepens Eye Research Institute, Harvard Medical School, 20 Staniford Street, Boston, MA, 02114
elsner@vision.eri.harvard.edu

http://color.eri.harvard.edu/annhom.htm

Abstract: Measurements of the human ocular fundus that make use of the light returning through the pupil are called reflectometry. Early reflectometry studies were limited by poor light return from the retina and strong reflections from the anterior surface of the eye. Artifacts produced misleading results in diseases like age-related macular degeneration. Novel laser sources, scanning, confocal optics, and digital imaging provide improved sampling of the signal from the tissues of interest: photoreceptors and retinal pigment epithelial cells. A wider range of wavelengths is now compared, including the near infrared. Reflectometry now provides functional mapping, even in severe pathology.

©2000 Optical Society of America

OCIS codes: (170.3880) Medical and biological imaging; (330.430) Noninvasive assessment of the visual system; (170.4470) ophthalmology

---

References, note, and links

1. F. C. Delori and K. P. Pflibsen, "Spectral reflectance of the human ocular fundus," Appl. Opt. **28,** 1061-1077 (1989).
2. A. E. Elsner, S. A. Burns, J. J. Weiter and F. C. Delori, "Infrared imaging of subretinal structures in the human ocular fundus," Vision Res. **36,** 191-205 (1996).
3. S. A. Burns, S. Wu, F. C. Delori and A. E. Elsner, "Direct Measurement of human cone photoreceptor alignment," J. Opt. Soc. Am. A **12,** 2329-2338 (1995).
4. A. E. Elsner, S. A. Burns, G. W. Hughes and R. H. Webb, "Reflectometry with a Scanning Laser Ophthalmoscope," Appl. Opt. **31,** 3697-3710 (1992).
5. S. Marcos, R.-P. Tornow, A. E. Elsner and R. Navarro, "Foveal cone spacing and cone photopigment density difference: objective measurements in the same subjects." Vision Res. **37**, 1909-1915 (1997).
6. A. E. Elsner, S. A. Burns, E. Beausencourt and J. J. Weiter, "Foveal cone photopigment distribution: small alterations associated with macular pigment distribution," Invest. Ophthalmol. Vis. Sci. **39**, 2394-2404 (1998).
7. A. E. Elsner, S. A. Burns, F. C. Delori and R. H. Webb, "Quantitative Reflectometry with the SLO," in *Laser Scanning Ophthalmoscopy and Tomography*, J. E. Nasemann and R.O.W. Burk eds. (Quintessenz-Verlag, Munich, 1990), pp. 109-121.
8. A. E, Elsner, S. A. Burns, M. R. Kreitz and J. J. Weiter, "New views of the retina/RPE complex: quantifying sub-retinal pathology," in *Noninvasive Assessment of the Visual System*, Vol, 1 of OSA Proceedings Series (Optical Society of America, Washington, D.C., 1991), pp. 150-153.
9. A. E. Elsner, D.-U. Bartsch, J. J. Weiter and M. E. Hartnett, "New devices in retinal imaging and functional evaluation," in *Practical Atlas of Retinal Disease and Therapy*, W. Freeman ed. (Lippincott-Raven, New York, 1998) 2nd edition, pp. 19-55.
10. L. M. Kelley, J. P. Walker, G. L. Wing, P. A. Raskauskas and A. E. Elsner, "Scanning laser ophthalmoscope imaging of age related macular degeneration and neoplasms," J. Ophthalmic Photography **3** 89-94 (1997).
11. M E. Hartnett and A. E. Elsner, "Characteristics of exudative age-related macular degeneration determined in vivo with confocal direct and indirect infrared imaging," Ophthalmol. **103**, 58-71 (1996).
12. L. V. Johnson, S. Ozak, M. I. Staples, P. A., Erickson and D. H. Anderson, "Potential role for immune complex pathogenesis in drusen formation," Exp. Eye Res. **70,** 441-449 (2000).
13. The longitudinal study and image of the first patient re-tested are at **http://color.eri.harvard.edu/annhom.htm**
14. A. E. Elsner, L. Moraes, C. W. Kunze and M. E. Hartnett, "Foveal cone photopigment distribution in age-related macular degeneration: association with fundus features," in *Vision Science and Its Applications*, Vol. 1 of OSA Proceedings Series (Optical Society of America, Washington, D.C., 1998) pp.14-17.

15. A. E. Elsner, A. Remky, E. Beausencourt and S. A. Burns, "A statistical method to quantify drusen in SLO images," in *Vision Science and Its Applications*, Vol. 1 of OSA Proceedings Series (Optical Society of America, Washington, D.C., 1996), pp. 268-271.
16. R.-P. Tornow and R. Stilling, "Scanning laser densitometry and color perimetry demonstrate reduced photopigment density and sensitivity in two patients with retinal degeneration" Vision Res. **39**, 3630-3641 (1999).
17. M. A. Sandberg, B. S. Pawlyk E. L. Berson, "Acuity recovery and cone pigment regeneration after a bleach in patients with retinitis pigmentosa and rhodopsin mutations," Invest. Ophthalmol. Vis. Sci. **40**, 2457-2461 (1999).
18. S. A. Burns, S. Wu, J. He, J and A. E. Elsner, "Variations in photoreceptor directionality across the central retina," J. Opt. Society Amer A **14**, 2033-2040 (1997).
19. P. J. DeLint, T. T. Berendschot and D. A. van Norren, "A comparison of the optical Stiles-Crawford effect and retinal densitometry in a clinical setting," Invest. Ophthalmol. Vis. Sci. **39**, 1519-1523 (1998).

Introduction

To compare changes in retinal structure and function, and corresponding subretinal structure, noninvasive imaging techniques have been developed. Reflectometry uses the light returning through the pupil of the eye from the human ocular fundus, which is comprised of layers of complex structures. In reflectometry, the signal is limited by the poor return of light from the complex structures, as well as the small solid angle of the exit pupil. The layers contain differing amounts and types of absorbing pigments with a wide variety of spectra, as well as large and small scale scattering bodies and polarizing elements(1-3). The distribution of absorbing and scattering bodies differs not only in anterior-posterior plane, but also across the fundus. An optical model of the fundus is inaccurate if the tissues are assumed to be either a mirror or a single, uniform scattering surface. Nor is spectroscopy successful, unless the target tissues can be carefully limited in spatial extent and the wavelength range controlled to minimize artifacts of the eye's chromatic aberration or from absorbing tissues. The different optical properties of the tissues help probe them in a noninvasive manner.

An established use of reflectometry is the quantification of photopigment, the light sensitive pigment contained within the photoreceptors. (Ref. 2 has a review). Photoreceptors provide the first step of vision, when light energy is changed to chemical energy. The amount of photopigment is quantified by comparing measurements before and after exposure to light sufficiently bright to bleach photopigment to a dilute concentration (2,4-6). Known as retinal densitometry, this technique can be performed with a single wavelength for both measurement and test. This simplifies the assumptions used previously for multi-spectral measurements, which required modeling over a range of wavelengths broad enough for differential effects of absorption for blood and melanin, and chromatic aberration.

A second example of reflectometry is the quantification of macular pigment. This pigment has no known direct role in the capture or transduction of light energy, but it is present in all normal retinas, most visibly in the central region of the retina called the macula. This pigment is physically associated with the photoreceptors and known to be comprised of two anti-oxidants: lutein and zeaxanthin. A reflectometry technique to quantify the spatial distribution compares the relative change over the fundus for two wavelengths that differ little in absorption for many of the main absorbing pigments such as melanin, but differ greatly in absorption by macular pigment (6-7). As macular pigment is at its highest concentration in the macula, it is necessary to bleach photopigment in the region so that the differences across the retina will not include the variation in photopigment coverage.

A third example of reflectometry is the quantification of subretinal structures such as drusen and hyperpigmentation, using infrared imaging and red imaging (2, 6-11). These are the hallmarks of pathological changes in age-related macular degeneration. Photoreceptors lie directly over and are in contact with the retinal pigment epithelium, which in turn contains or lies over or under these pathological structures. Drusen and hyperpigmentation occur with normal aging, although they are difficult to detect (8-11). By careful control of wavelength

and imaging mode, it is possible to emphasize one type of structure, rendering the others relatively invisible. This is particularly important for visualizing subretinal structures, which are obscured with conventional photography by structures returning a relatively large proportion of the light, e.g. the vitreoretinal interface or reflective structures in the retina.

Advances in photonics provide improvement over earlier techniques. Laser scanning illuminates one spot at a time, minimizing unwanted light from other structures (4). Confocal imaging allows the use of apertures in a plane conjugate to the sample, helping control the origin of light reaching the detector. Digital imaging allows the monitoring and correction of eye position, plus numerous data analysis options: summing or averaging of images, subtraction of pairs of images, ratio measurements of images, and comparison of a reference and a standard region of interest in a single image (2,7).

Method

apparatus

The research Scanning Laser Ophthalmoscope (SLO) and image acquisition system are used for all three types of data collection: retinal densitometry, macular pigment measurements, and infrared or red imaging (2,4,6). This instrument differs from commercial models in several ways important for quantitative results. There are eight laser sources. Three are unique for this application: a 594 nm HeNe (Research Electro-optics, Boulder, CO), an 830 nm laser diode with beam shaping (Liconix, Santa Clara, CA), and an infrared laser (Chr:Li:SaF, EyeScan, Schwartz Electro-optics, Concord, MA) tunable to 810-860 nm. This is the first imaging instrument to utilize this source. The power of the illumination beam can be rapidly adjusted over a continuous range. Lasers used for quantitative measurements are calibrated prior to each experiment, using a photometer (EG&G, DR-2550, San Diego, CA). Each HeNe or Argon laser is adjusted using neutral density filters and an analog acousto-optic modulator. The infrared lasers have 3-log-unit neutral density wedges. The Argon (Uniphase, San Jose, CA) wavelengths are made monochromatic with interchangeable, 6-cavity interference filters, centered on the laser line at either 488 or 514 nm. The laser beam path lengths are at least 1 m long prior to the entrance aperture of the instrument, permitting beam shaping, collimation, and spatial filtering. There are two types of confocal apertures: a) pinhole apertures of 100 microns or larger with respect to the retina, producing direct mode images and b) annular apertures with central stops of 100 microns or larger, producing indirect mode images.

A clinical scanning laser ophthalmoscope (Rodenstock, Ottobrunn-Riemerling, Germany) is being used in a longitudinal study of 100 patients with age-related macular degeneration, the family members, and over 120 age-matched control subjects at the Retina Consultants of SW Florida. This instrument has the typical three laser sources: a 633 nm HeNe, an Argon with 488 and 514 nm, and a 790 nm diode laser. It lacks mirror pairs on both the Argon and diode lasers for precision alignment with respect to the confocal aperture. Indirect mode images are possible only with the HeNe.

photopigment

To map the foveal cone photopigment distribution, we used the method developed previously for the long wavelength sensitive (LWS) and middle wavelength sensitive (MWS) cone types (2,4). Following 15 min of dark adaptation and alignment to the instrument with infrared light, the subject's fundus was imaged with a 594 nm HeNe illumination source at 94 microwatts to produce 5.4 log td. Images were digitized for the 28.6 x 23.0 deg field, continuously after first exposure to the bright light, then at 1, 2, 3, and 4 min later. This intensity is sufficient to bleach photopigment of both the long- and medium- wavelength sensitive cone types to a steady-state dilute concentration, even in older subjects. The foveal cone photopigment density difference (DD) is computed digitally from aligned images as

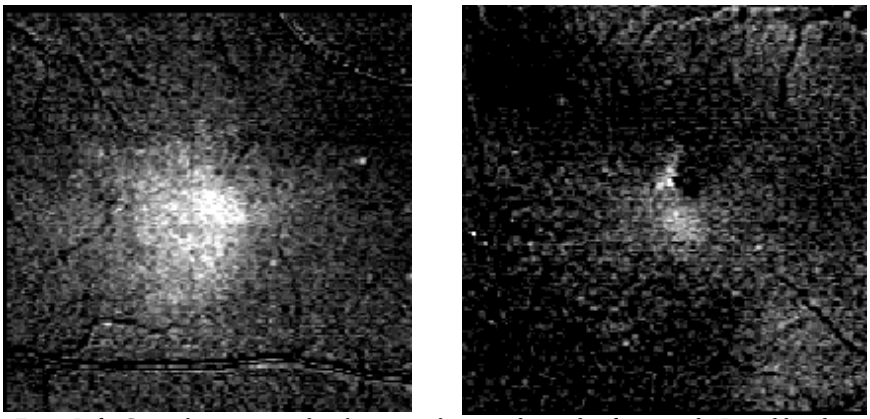

Fig. 1 Left- Cone photopigment distribution in the central macula of a normal 45 yr old male subject. Right- Cone photopigment distribution of a normal 35 year old female, showing a defect in a smooth distribution.

$$DD = \log(\text{bleached image}) - \log(\text{dark adapted image}). \quad (1)$$

macular pigment

The differences among subjects in the distribution of macular pigment were investigated with a reflectometry technique that is objective and resistant to stray light (6,7). The main assumption is that the macular pigment absorption causes the difference in the distribution of light returning from the macula at 488 vs. 514 nm, after the cone photopigment is bleached. When these wavelengths are used, other ocular pigmentation, such as melanin, produces less artifact than when both short and long wavelength data are used in one measurement. The power, alignment, and focus were adjusted for each wavelength to reduce artifacts from the foveal reflex, and to maximize the use of grayscale in the macula for digital image processing. The maximum power did not exceed 50 microwatts. The double density is computed as

$$MDD = \log(\text{image at } 514\text{nm}) - \log(\text{image at } 488\text{nm} * c) \quad (2)$$

and c is the ratio of 514 to 488 nm for a 10 x 10 pixel region of interest 7 - 9 deg eccentric.

infrared imaging and red imaging

The subretinal structures are better visualized by using these longer wavelengths. In Boston, infrared wavelengths and 633 nm were used with both pinhole and annular apertures, providing images based on directly backscattered (direct mode) or multiply scattered light (indirect mode), respectively. Young subjects with defects in their photopigment distributions were imaged again to determine if the source of the artifacts corresponded to subretinal damage, reflections, or other biological sources. In Ft. Myers, direct infrared and indirect red images were acquired and transmitted digitally to Boston for processing (Topcon Imagenet).

Results

The functional map of photopigment in the area of central vision is readily obtained (Fig. 1). Young, healthy subjects have a distinct peak of photopigment centered in the fovea, but older subjects have alterations from the ideal distribution (6). Distinct focal detects are found, offset from and larger than those that result from the artifact of the foveal reflex. A defect in photopigment distribution implies abnormal cone outer segments or missing cones. These defects can be clearly seen in all the visible wavelength images, and the position depends upon the prominent absorbing pigments at each test wavelength. For 594 nm, the main

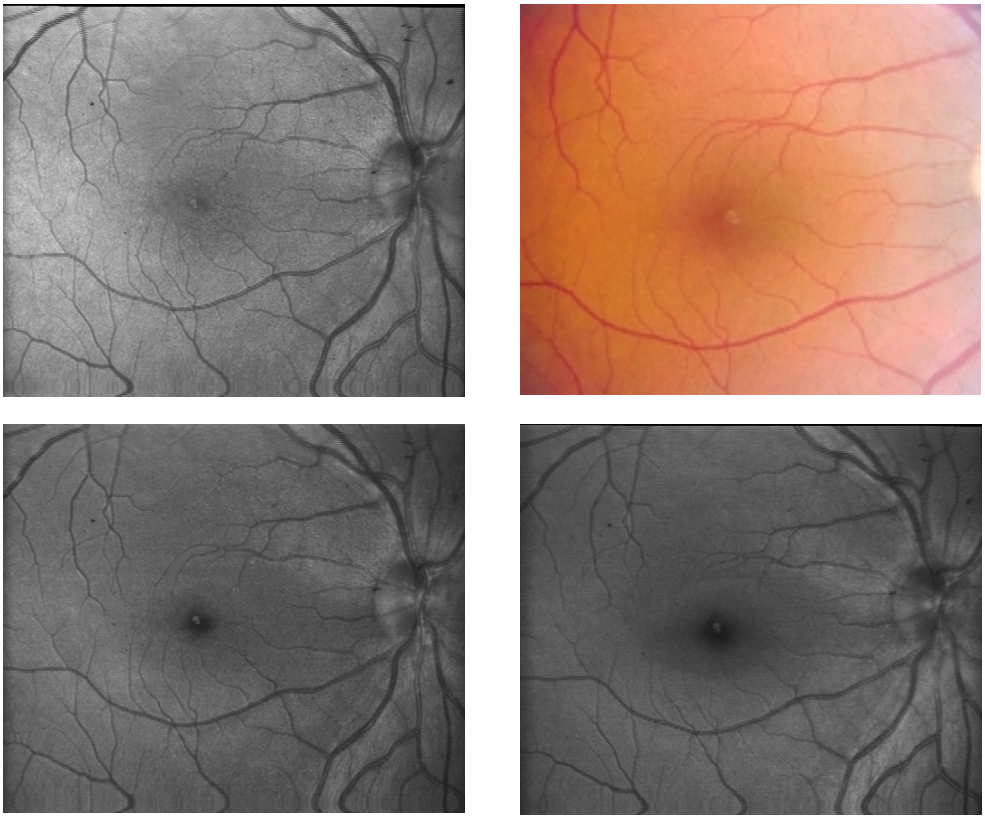

Fig 2. Top left- Image of female subject in Fig 1, with a 594 nm, 40 deg field. The bright detect that corresponds to the missing photopigment. Note that this wavelength localizes retinal vasculature, but not macular pigment. Top right- color fundus photograph. Bottom left- 514 nm, 40 deg field, showing little the defect, but little absorption of macular pigment at this wavelength . Bottom right- 488 nm, 40 deg field. The dark central region indicates the location of macular pigment.

absorbing pigment is blood, once the photopigment is bleached. The image at this wavelength shows a punctate defect (Fig. 2), similar to the defect in this subject's color fundus photograph. While the defects of many subjects are so small as to be unnoticeable in clinical examination, nevertheless they may provide interesting clues as to how the retinal structure changes with the influences of disease or aging. The image at 514 nm also contains a relatively punctate defect (Fig. 2). At this wavelength the main absorbing pigment is also blood, although there is an increase of melanin absorption compared with the 594 nm and longer wavelength data. However, at 488 nm, the defect is noticeably larger and offset somewhat. The main absorbing pigment at this wavelength is potentially macular pigment, although there is absorption by blood and melanin. The macular pigment distribution, calculated from the 488 and 514 images, also has a defect in the center (Fig. 3). As macular pigment is found in tissues typically displaced from the central fovea, such as cone axon segments, then the defects are expected to spatially correspond with some slight differences.

Infrared imaging and red imaging

Infrared light, and to a lesser extent red light, passes readily through melanin that is evenly distributed, and through thin layers of blood. This reveals subretinal structures in patients with age-related macular degeneration (Fig 4) that are present to a much lesser extent in normal subjects (Fig. 3). Drusen (dense lipoprotein) (12) and hyperpigmentation (clumped melanin and integrated compounds) seen with the scanning laser methods have been shown to

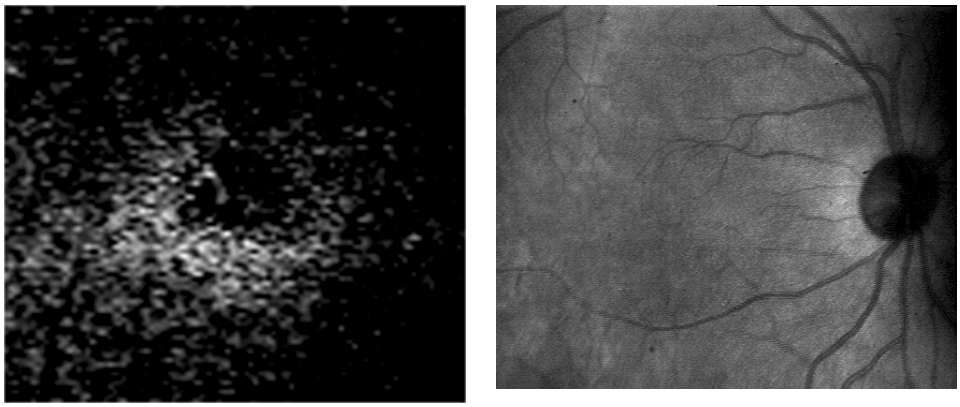

Fig. 3. Left- Macular-centered image of a small retinal defect of macular pigment, computed from the images in Fig. 2 and magnified 5X. The contrast is adjusted to enhance the print visualization of the macular pigment. Right- 860 nm, 40 deg image. No large drusen or clumped hyperpigmentation were seen in any normal subject that co-localized with the measured alterations in photopigment or macular pigment distribution.

correlate with good quality clinical photography and angiography. Both these types of pathology indicate serious damage to the structure and function of retinal pigment epithelial cells, the metabolic support cells for photoreceptor outer segments.

The new techniques allow the *in vivo* testing of models of aging and disease pathophysiology. We have two important findings. First, there are alterations with aging and across locations in an eye of the distributions of both photopigment and macular pigment, occurring in normal subjects with no sign of corresponding subretinal disease. Comparison of Figs. 1-3 shows that the subject has limited photopigment and macular pigment in a small region near the central macula, but no signs of drusen or hyperpigmentation beneath this region. There is mild hyperpigmentation in a spatially separate region. This apparently rules out the possibility that all damage to cones proceeds from damage to the retinal pigment epithelium.

Second, there was damage to the central region in the majority of eyes of our patients with age-related macular degeneration, long before the visual acuity dropped below 20/20. These types of damage, seen with infrared and red imaging techniques in Figs. 4 and 5, are related to more traditional ones for a wide range of subjects and patients (2,11,13-15). Of the first 100 patients with red imaging that permitted visualization of hyperpigmentation, but who did not have significant atrophy in the central macula, 47 patients had visual acuity of 20/20 or better. Yet 19 of these had clumped hyperpigmentation that was visualized in the central 3000 microns around fixation, as seen on the right side of Fig. 4. The dark pigment figures indicate severe damage to the retinal pigment epithelium. While 47 of the 100 patients had clumped hyperpigmentation in the central 3000 microns, only 2 of 98 normal subjects of comparable age had clumped hyperpigmentation ($p < 0.0001$, Chi-square (1)). For this same patient population, we have previously shown two ways to quantify drusen, which appear as bright spots on the left side of Fig. 4 (15). The drusen typically cover a readily quantifiable portion of the central macula, where rods are not most numerous. Image fusion shows the relative retinal locations of the two types of damage, drusen and hyperpigmentation (Figs. 5). A longitudinal study of these patients with age-related macular degeneration is ongoing, with 60 patients retested to date in Ft. Myers, FL (13), along with new patients and controls.

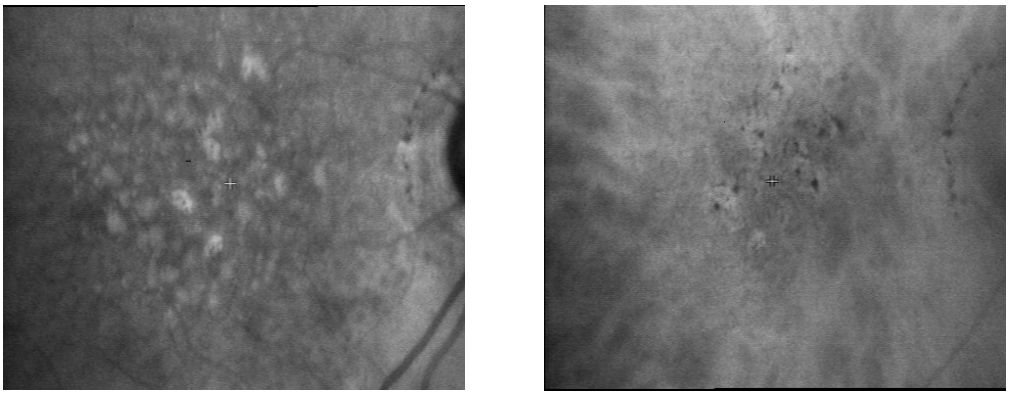

Fig. 4. Left- Infrared image of the macula of a patient with age-related macular degeneration. The large, bright structures are drusen. Right- Red image of the same patient. The dark structures are hyperpigmentation.

Discussion

Functional mapping of cone photopigment distribution and macular pigment distribution visualized defects in the supposedly normal eyes, long before any clinical signs of age-related macular degeneration are found in the normal population. These changes could be a part of the aging process of the eye, or signify preceding pathology.

We have shown new reflectometry data for aging and early age-related macular degeneration. Previously, we reported that the cones in the central macula have little photopigment in age-related macular degeneration, even in patients with good visual acuity (14). Other recent reflectometry publications include quantifying photopigment regeneration in patients with retinitis pigmentosa (16,17). A new method used photoreceptor alignment reflectometry to estimate cone photopigment density by the guided light before vs. after a

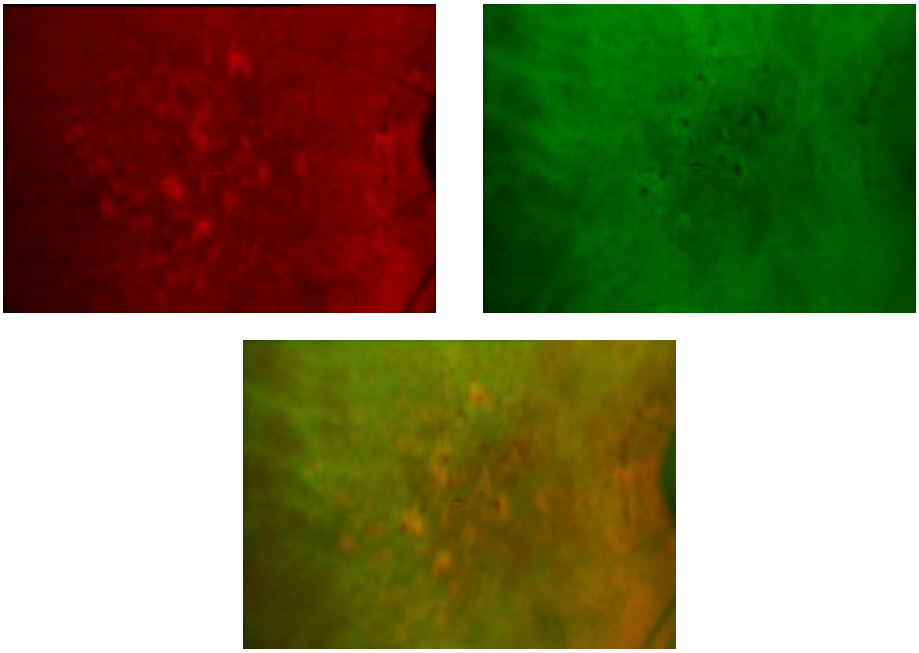

Fig. 5. Pseudo color from images in Fig 4, to show image fusion. Top left- confocal image. Top right- multiply scattered light image. Bottom- fusion image.

strong bleach (3,18). Photoreceptor alignment may also be used to determine the distribution of light guidance across the retina (3,18,19).

Acknowledgements
Supported by EYO7624, EYO3790, DE-FG 02-91ER61229, Lions Club of Massachusetts, Chartrand Foundation. We thank Topcon and Mr. Anthony Pugliese for the use of ImageNet.